

Early Paleocene Paleoceanography and Export Productivity in the Chicxulub Crater

Christopher M. Lowery^{1*}, Heather L. Jones², Tim Bralower², Ligia Perez Cruz³, Catalina Gebhardt⁴, Michael T. Whalen⁵, Elise Chenot⁶, Jan Smit⁷, Marcie Purkey Phillips¹, Konstantin Choumiline⁸, Ignacio Arenillas⁹, Jose A. Arz⁹, Fabien Garcia¹⁰, Myriam Ferrand¹⁰, Johanna Lofi⁶, Sean P.S. Gulick¹, Exp. 364 Science Party¹¹

¹Institute for Geophysics, Jackson School of Geosciences, University of Texas at Austin, USA

²Department of Geosciences, Pennsylvania State University, University Park, USA

³Instituto de Geofísica, Universidad Nacional Autónoma De México, Ciudad de México, México

⁴Alfred Wegener Institute Helmholtz Centre of Polar and Marine Research, Bremerhaven, Germany

⁵Department of Geosciences, University of Alaska Fairbanks, USA

⁶Géosciences Montpellier, Université de Montpellier, France

⁷Faculty of Earth and Life Sciences (FALW), Vrije Universiteit Amsterdam, Netherlands.

⁸Department of Earth Sciences, University of California Riverside, USA

⁹Departamento de Ciencias de la Tierra and Instituto Universitario de Investigación en Ciencias Ambientales de Aragón, Universidad de Zaragoza, E-50009, Spain

¹⁰Biogéosciences, Université de Bourgogne Franche-Comté, France

¹¹See Appendix 1

Corresponding author: Christopher Lowery (cmlowery@utexas.edu)

Key Points (three, 140 characters each)

- Export productivity in the Chicxulub crater is high for the first 300 kyr after the K-Pg boundary
- Water column stratification is variable for the first ~Myr of the Paleocene; changes in stratification associated with nannofossil turnover
- Many other sites show similar changes ~65.7 Ma, suggesting global change in circulation possibly linked to the coeval Dan-C2 hyperthermal

28 **Abstract**

29 The Chicxulub impact caused a crash in export productivity in much of the world's oceans which
30 contributed to the extinction of 75% of marine species. In the immediate aftermath of the extinction, local
31 export productivity was highly variable, with some sites, including the Chicxulub crater, recording
32 elevated export production. The long-term transition back to more stable export productivity regimes has
33 been poorly documented. Here, we present elemental abundances, foraminiferal and calcareous
34 nannoplankton assemblage counts, total organic carbon, and stable carbon isotopes from the Chicxulub
35 crater to reconstruct long-term changes of productivity over the first 3 Myr of the Paleocene. We show
36 that export production was high for the first 300 kyr of the Paleocene and then declined for the next 700
37 kyr. This decline is broadly associated with increasing water column stratification. A final decrease in
38 export productivity occurred after ~ 1 Myr. We suggest that increasing upper water column stratification
39 reduced the availability of nutrients in the photic zone, which drove an increase in the efficiency of the
40 biological pump. Increased pump efficiency created a positive feedback which drove the further
41 development of oligotrophic conditions; the onset of oligotrophy perturbed the stable disaster
42 nannoplankton assemblage and allowed other taxa to gain a foothold in the ecosystem. The initial decline
43 in export productivity 300 kyr after the boundary is observed across the globe and may have been an
44 important driver of turnover in post-extinction communities. We postulate that these changes are related
45 to the Dan-C2 hyperthermal event.

46 **Plain Language Summary**

47 The end Cretaceous mass extinction was caused by the impact of an asteroid on the modern Yucatán
48 Peninsula, Mexico. The impact ejected aerosols and dust into the air that blocked out the sun, causing a
49 severe decline in photosynthesis and the collapse of marine food webs. However, the change in the
50 amount of food created by photosynthesizing plankton that makes it to the seafloor (export productivity)
51 was not temporally or spatially uniform across the oceans. At some places, including the Chicxulub
52 crater, export productivity was actually high immediately after the impact. We produced an extended ~3

53 million year record of export productivity in the crater to determine how long it remained high and why it
54 eventually declined. Export production was very high for the first 300,000 years after the impact and
55 remained elevated for the next 700,000 years. It eventually declined due to changes in mixing in the
56 surface ocean which affected how efficiently nutrients were removed from the surface ocean to the deep
57 sea. This decline caused a change in the population of fossilized primary producers from a few species
58 adapted to high nutrient, high productivity conditions to a diverse population better adapted for low
59 nutrient, low productivity conditions.

60 **Keywords:** K-Pg, Chicxulub Crater, Paleoproductivity, Foraminifera, Nannoplankton, Paleocene, Dan-
61 C2 Hyperthermal

62 **1. Introduction**

63 At the end of the Cretaceous Period (~66 Ma), the impact of an asteroid on the Yucatán platform
64 in the southern Gulf of Mexico caused the extinction of 75% of species on Earth, including ~90% of
65 pelagic calcifiers such as planktic foraminifera and calcareous nannoplankton (Alvarez et al., 1980; Smit
66 et al., 1980; Hildebrand et al., 1991; Jablonski, 1995; Schulte et al., 2010, Fraass et al., 2015; Knoll and
67 Follows, 2016). Dust and sulfate aerosols ejected from the carbonate and evaporite-rich target rock, as
68 well as soot from possibly global wildfires, blocked the sun, resulting in severe short-term cooling
69 (Vellekoop et al., 2014, 2016; Bardeen et al., 2017 Brugger et al., 2017; Artemieva et al., 2017; Gulick et
70 al., *in press*) and collapse of the food chain due to a sharp decline in photosynthesis (Zachos et al., 1989;
71 D'Hondt et al., 1998; Kring, 2007). These effects were short-lived, however, as most dust, soot, and
72 aerosols were removed from the atmosphere on the order of years (Brugger et al., 2017), and the oceans
73 quickly became hospitable, even at ground zero in the Chicxulub crater (Lowery et al., 2018).

74 The recovery of marine primary productivity was a crucial first step in the overall recovery of the
75 ocean ecosystem after this apocalypse. Understanding this process has long been a goal of researchers
76 interested in the recovery of life after major mass extinctions (e.g., Hsü and McKenzie, 1985). Early

77 records of productivity after the Cretaceous-Paleogene (K-Pg) mass extinction derived from carbon
78 isotopes show that the vertical gradient of $\delta^{13}\text{C}$, developed by the export of organic carbon from the
79 surface ocean to the seafloor, collapsed in the early Danian for about 1.8 Myr (Hsü and McKenzie, 1985;
80 Zachos et al., 1989; D'Hondt and Zachos, 1998; Coxall et al., 2006; Birch et al., 2016). This was initially
81 interpreted as evidence of complete or nearly complete cessation of surface ocean productivity, an idea
82 which became known as the Strangelove Ocean (Hsü and McKenzie, 1985). Later, D'Hondt et al. (1998)
83 suggested that surface ocean productivity continued but that the disappearance of larger organisms
84 prevented the export of organic matter to the deep sea (known as the Living Ocean hypothesis). The
85 observed changes in the carbon isotope gradient can be explained by a small increase in the percentage
86 (e.g., from 90 to 95%) of the organic matter that is remineralized in the upper ocean (D'Hondt et al.,
87 1998; Alegret et al., 2012).

88 There is a great deal of data indicating continued organic carbon flux to the deep sea in the early
89 Danian. Benthic foraminifera, which are entirely dependent on the flux of organic matter from above for
90 food, did not suffer extinction at the K-Pg boundary (Culver, 2003; Alegret et al., 2012). Biogenic
91 barium, a paleoproductivity proxy which has been shown to correlate with organic matter flux from
92 overlying surface water, i.e., *export* productivity (e.g., Griffith and Paytan, 2007), indicates that export
93 production did not uniformly decline across the oceans, as some sites actually show an increase in export
94 the period after the Chicxulub impact (Hull and Norris, 2011). Broadly, sites in the Gulf of Mexico/North
95 Atlantic/Tethys region record reduced export production in the early Danian (Alegret et al., 2001;
96 Esmerly-Senlet et al., 2015; Vellekoop et al., 2017), whereas sites in the central Pacific record increased
97 export production during the same time period (Hull and Norris, 2011). This geographic heterogeneity
98 was proposed to be driven by the uneven distribution of toxic metals in the ocean, related to distance from
99 the Chicxulub crater and the angle of the impact, interpreted to be from south to north (Jiang et al., 2010).
100 However, new modelling based on geophysical datasets and results from recent International Ocean
101 Discovery Program/International Continental Drilling Program (IODP/ICDP) joint Expedition 364, which

102 drilled the peak ring of the Chicxulub crater (Morgan et al., 2017), has found that the angle of impact was
103 steeply inclined and that the direction was towards the southern hemisphere (Collins et al., in review;
104 Lowery et al., 2019). Moreover, cores taken just above the impact-generated rocks show evidence of the
105 rapid establishment of a healthy, high-productivity ecosystem in the crater within 30 kyr of the impact
106 (Lowery et al., 2018). This was an order of magnitude quicker than the recovery of export productivity at
107 other Gulf of Mexico/North Atlantic sites, which suggests that differences in marine productivity were
108 not driven by distance from the crater, impact direction, or linked environmental factors. Rather, it
109 appears that this post-impact heterogeneity must be controlled by more seemingly “random” ecological
110 factors like incumbency and competitive exclusion (Hull et al., 2011; Schueth et al., 2015; Lowery et al.,
111 2018).

112 It is unclear how long high export productivity persisted at ground zero, and how it relates to
113 global patterns of heterogeneous export production in the early Danian. Was this locality
114 oceanographically pre-disposed to high export productivity, or did changing conditions eventually lead to
115 a decline? If so, what conditions shifted to cause lower export production?

116 The answers to these questions, particularly the cause of the shift from heterogeneous post-impact
117 export productivity regimes to whatever succeeded them, also have important bearing on our
118 understanding of the biological recovery after the Chicxulub impact. Perhaps surprisingly, given the rapid
119 recovery of export productivity and the high diversity of planktic foraminifera, the recovery of calcareous
120 nannofossil diversity was delayed within the Chicxulub crater. Disaster taxa, including cyst-forming
121 dinoflagellates such as *Cervisiella* (a genus previously known as *Thoracosphaera*) and the eutrophic
122 nannoplankton *Braarudosphaera*, dominated nannofossil assemblages for a million years after the K-Pg
123 boundary (Jones et al., 2019). Ecological experimentation, exemplified by a series of acmes of taxa which
124 rapidly increased then declined in abundance (“boom-bust successions”), began ~ 1 Myr after the impact
125 (Jones et al., 2019), well after similar successions at other sites had subsided (e.g., Bown, 2005; Schueth
126 et al., 2015). Jones et al. (2019) attributed the persistence of disaster species within the Chicxulub crater

127 to high productivity for the first million years of the Paleocene. These disaster taxa were better adapted to
128 high nutrient conditions, and thus likely outcompeted other calcareous phytoplankton until nutrient
129 concentrations began to decline, at which point a more diverse ecosystem was slowly established via
130 boom-bust successions. Export productivity and photic zone nutrient concentrations are thus believed to
131 be fundamental to ecological recovery (Jones et al., 2019). Understanding the timing and driver(s) of
132 changes in export productivity is essential to constrain the fundamental controls on the early recovery of
133 phytoplankton diversity.

134 There are a number of environmental changes which may have influenced changes in export
135 productivity in the early Danian. Deccan volcanism began in the Maastrichtian and continued until
136 approximately 65.6 Ma (Schoene et al., 2019) to 65.4 Ma (Sprain et al., 2019), or 400 kyr to 600 kyr after
137 the boundary. Environmental effects of Deccan volcanism have been proposed as a mechanism to delay
138 the recovery of life following the K-Pg mass extinction (e.g., Gertsch et al., 2011; Renne et al., 2015;
139 Punekar et al., 2014a,b), although it is often unclear what is meant by “recovery.” Lowery and Fraass
140 (2019) found no relationship between the recovery of planktic foraminifer species diversity and the “main
141 phase” of Deccan volcanism (or its subsequent termination) in the earliest Danian. Perhaps Deccan
142 volcanism instead exerted some influence on the recovery of export productivity. Meanwhile, the first
143 Paleogene hyperthermal event occurred a mere 300 kyr after the K-Pg boundary. The Dan-C2
144 hyperthermal is characterized by two negative carbon isotope excursions coincident with a similar double
145 spike in clay content and Fe content, and decrease in Ca in deep sea cores (Quillévéré et al., 2008;
146 Coccioni et al., 2010). Each excursion lasts ~40 kyr and they are separated by ~100 kyr, which Quillévéré
147 et al. (2008) interpreted as evidence of an orbital driver. Whatever the root cause, this event clearly had an
148 effect on marine ecosystems, altering assemblages of foraminifera and calcareous nannoplankton and
149 possibly driving eutrophication, shoaling of the lysocline, and deoxygenation (Coccioni et al., 2010). Was
150 the Dan-C2 also responsible for changes in export production?

151 Here, we examine planktic and benthic foraminifera, calcareous nannoplankton, and major,
152 minor, and trace elements to reconstruct export productivity, water column stratification, terrigenous flux,
153 and phytoplankton population change during the early Paleocene interval (66.0-62.5 Ma) of IODP Site
154 M0077 in the Chicxulub crater (Figure 1). These data are used to determine how long export productivity
155 remained elevated and if its eventual decline is due to changing environmental conditions. We then
156 compare our data from Chicxulub to coeval sites spanning the Paleocene oceans.

157 **2. Material and Methods**

158 In 2016, IODP/ICDP Expedition 364 drilled the peak ring (e.g., Morgan et al., 2016) of the
159 Chicxulub crater (Morgan et al., 2017), coring over 100 m of post-impact Paleogene sediments with
160 nearly 100% recovery. Ten meters of Paleocene pelagic carbonates were recovered at the base of the post-
161 impact section, conformably overlying the top of the impact breccia. The uppermost 40 cm of this interval
162 is cut by four disconformities and spans the middle and late Paleocene; the rest of the section, the focus of
163 this study, spans the earliest to middle Paleocene, and is continuous from 66 to ~62 Ma (Morgan et al.,
164 2017). Planktic foraminiferal and calcareous nannofossil samples were taken from identical depths
165 throughout the core and prepared using standard techniques. To obtain elemental abundance data, cores
166 were scanned on the AVAATECH XRF Core Scanner II at the University of Bremen. Total organic
167 carbon (TOC) and bulk rock stable carbon isotopes were also measured using standard techniques. Please
168 see supplemental information for full discussion of the analytical techniques employed here.

169 **2.1 Age Model**

170 The age model used here (Table 1) is a slightly updated version of that produced by the
171 Expedition 364 Science Party (Gulick et al., 2017). Calcareous nannofossil age determination is based on
172 the CP zonation scheme of Okada and Bukry (1980) following the taxonomic concepts of Perch-Nielsen
173 (1985) and Bown (1998). Planktic foraminifer biostratigraphy is based on the P zones of Berggren and
174 Pearson (2005) as modified by Wade et al. (2011), following the taxonomic concepts of Olsson et al.

175 (1999) and Pearson et al. (2006). Key taxa are illustrated in Figure 2. Calibrated ages assigned to each
176 datum are those reported in Appendix 3 of the Geologic Time Scale 2012 (Gradstein et al., 2012).
177 Because calcareous nannoplankton are poorly preserved at Chicxulub and form diachronous acmes
178 following the K-Pg mass extinction (Jones et al., 2019), zonal markers are either absent or inconsistent
179 with the planktic foraminifer datums. For this reason, we only used the planktic foraminifer biozones to
180 construct the age model (Table 1). Paleomagnetic reversals are not included in the age model because a
181 heterogenous chemical remnant re-magnetization occurred throughout the study interval obscuring the
182 original polarity (Morgan et al., 2017; Gulick et al., *in press*).

183 **3. Results and Discussion**

184 **3.1 M0077 Sedimentology and Terrigenous Flux**

185 The Paleocene interval at Site M0077 is primarily pelagic carbonate with varying degrees of
186 dilution by terrigenous material (Figure 3). We reconstruct terrigenous flux using several elemental
187 proxies and magnetic susceptibility (Figure 3). Iron is generally correlated with terrigenous sediments,
188 while calcium is primarily sourced from marine calcifiers. Both Fe and Ca are often used to infer
189 carbonate dissolution in deep sea cores, particularly during the Paleogene, which was characterized by
190 discrete episodes of CO₂ release, warming, and ocean acidification (Bralower et al., 2002; Edgar et al.,
191 2007; Quillévéré et al., 2008; Coccioni et al., 2010). However, we conclude that Fe and Ca variations are
192 driven by changes in dilution rather than dissolution because: (1) Site M0077 is relatively shallow, around
193 700 m water depth in the Paleocene (Lowery et al., 2018), well above the early Paleocene lysocline; and
194 (2), intervals of elevated Fe/depressed Ca do not correspond to intervals of reduced foraminifer
195 preservation (Figure 4). Core material at Site M0077 is strongly lithified, and had to be broken down with
196 a mortar and pestle prior to soaking. An unfortunate side effect of this aggressive disaggregation is the
197 fracturing of some fraction of the foraminifera. We did not distinguish foraminifera broken in this way
198 from fragments of foraminifera which may have experienced partial dissolution on the seafloor due to
199 deposition below the lysocline, a common proxy for ocean acidification (“Foram Fractionation Index;”

200 Thunell 1976). In order to establish some quantitative proxy for foraminifer preservation, we instead
201 report the number of individuals in each counted population that could not be identified to the genus level.
202 These “planktic spp.” are excluded from population analysis (other than planktic/benthic ratio) but
203 provide a useful approximation of preservation, with more unidentifiable individuals indicating worse
204 preservation. There is a slight positive correlation between Fe and preservation, and a corresponding
205 negative correlation between Ca and preservation (Figure 4). Enhanced preservation in carbonate-poor
206 intervals is likely due to dilution of the pure pelagic carbonate by clay (marls and organic-poor shales
207 generally contain the best-preserved fossils), and thus increases in Fe are interpreted to represent
208 terrigenous flux.

209 A number of trends in terrigenous flux are evident in the Paleocene interval of Site M0077
210 (Figure 3). Overall, terrigenous flux was low for the first ~ 1 Myr of the Danian and higher thereafter.
211 Numerous shorter peaks are superimposed on this long-term trend. The base rate of terrigenous flux,
212 particularly in Fe, is elevated in the upper part of the record relative to the low points around 615.6 mbsf
213 (65.4 Ma) and the base of the pelagic limestone. It should be noted that the closest land was > 500 km
214 away in modern central Mexico (Gulick et al., *in press*), and thus terrigenous material transported to Site
215 M0077 was dominated by clay that only slightly diluted the pelagic carbonate. Increases in the
216 terrigenous component, however, are a useful proxy for changes in continental weathering in the Gulf of
217 Mexico basin and likely indicate increased riverine flux, which we postulate drove changes in
218 stratification.

219 **3.2 M0077 Export Productivity**

220 Biogenic barium, primarily preserved in marine sediments as barite (BaSO_4), strongly correlates
221 with modern export production (Dymond et al., 1992; Francois et al., 1995; Eagle et al., 2003; Paytan and
222 Griffith, 2007) and is thus a commonly used export productivity indicator (e.g., Payton et al., 1996; Bains
223 et al., 2000; Griffith and Paytan, 2012), including in the early Paleocene (Hull and Norris, 2011). Barite is
224 primarily formed in marine environments during the remineralization of sinking organic matter, but it can

225 also be sourced from terrigenous sediments. Therefore, to isolate the biogenic fraction, barium is
226 normalized to the terrestrially-sourced element titanium (Dymond et al., 1992; Payton and Griffith, 2007).
227 Different continental drainage basins may have differing Ba/Ti ratios, and thus long-term changes in
228 sediment source area or dust vs. riverine flux may bias the data by indicating apparent changes in export
229 productivity (Payton and Griffith, 2007). However, significant changes in the sediment source to the
230 southern Gulf of Mexico did not occur until the Laramide Orogeny, which began in the late Paleocene
231 and therefore would not have influenced early Paleocene sedimentation (Galloway et al., 2000). Because
232 there is also not a major long-term change in sediment type (pelagic carbonate) over the interval studied
233 here, we consider sedimentary source changes to be an unlikely driver of observed trends in biogenic
234 barium. To test this interpretation, we compare the Ba/Ti export productivity proxy to several other
235 productivity proxies, specifically planktic foraminifer assemblage changes and benthic foraminiferal
236 abundance.

237 Paleocene planktic foraminifera exhibit several adaptations in their trophic strategies, which
238 allow some groups to thrive in low-nutrient environments. Microperforate and smooth normal perforate
239 planktic foraminifera (*Guembelitra*, *Globoconusa*, *Parvularugoglobigerina*, *Woodringina*,
240 *Chiloguembelina*, etc.) were grazers, feeding on phytoplankton and any organic detritus that they could
241 catch in their network of rhizopodia. Their food sources did not include most motile zooplankton, which
242 are generally able to free themselves from such unsupported rhizopodal networks (Hemleben et al., 1991).
243 In the early Danian, however, some new genera (*Eoglobigerina* and the Subbotinids) evolved spines, long
244 protrusions of calcite which provide an anchor for the rhizopods and allow them to hold on to motile prey,
245 enabling these groups to adapt a carnivorous lifestyle and open a new food source: other zooplankton
246 (Hemleben et al., 1991; Olsson et al., 1999). Several million years later, another group of planktic
247 foraminifera acquired photosymbionts, beginning with *Praemurica uncinata* and followed by *Acarinina*,
248 *Morozovella*, and *Igorina* (Coxall et al., 2006). In the modern ocean, photosymbiont-bearing planktic
249 foraminifera tend to dominate in oligotrophic subtropical gyres. Spinose and symbiont-bearing planktic

250 foraminifera are thus better adapted to food-limited environments, and we expect them to be predominant
251 in oligotrophic waters. On the other hand, non-spinose, non-symbiont bearing planktics, the grazers, are
252 best adapted to eutrophic environments, and should be dominant there.

253 Benthic foraminifera are also powerful paleoenvironmental indicators. They are primarily
254 sensitive to changes in dissolved oxygen and food supply, with fewer benthics in dysoxic or oligotrophic
255 environments (Jorissen et al., 1995; Gooday, 2003; Van Hinsbergen et al., 2005). Benthic abundance is
256 also often inversely correlated with water depth (e.g., Murray, 1976; Culver, 1988; Van der Zwaan et al.,
257 1990; Leckie and Olson, 2003). The seafloor at Site M0077 was clearly well-oxygenated throughout the
258 study interval, as evidenced by abundant ichnofauna (Morgan et al., 2017). Additionally, the site was
259 located in upper/middle bathyal depths (600-700 m; Gulick et al., 2008; Lowery et al., 2018), and low-
260 amplitude sea level change throughout the early Paleocene (Kominz et al., 2008) should not have affected
261 the %benthics at this depth. With changes in oxygen and sea level thus ruled out, we are confident that
262 food supply to the seafloor (i.e., export production) was the strongest influence on %benthics at Site
263 M0077.

264 Export productivity was high overall in the early Danian, and broadly declined from 66.0 to ~64.5
265 Ma (616.5 to ~613.7 mbsf), based on Ba/Ti, %benthics, and planktic trophic groups (Figure 5). Ba/Ti
266 ratios, the highest resolution dataset, show that the interval of highest export productivity terminated
267 sharply around 65.7 Ma (616.2 mbsf). This time interval corresponds to the Dan-C2 hyperthermal
268 (Quillévére et al., 2008; Coccioni et al., 2010); unfortunately, low sedimentation rates, extensive
269 bioturbation, and diagenetic alteration (expressed as stylolites in the core) mean that the carbon isotope
270 excursion for this hyperthermal is not preserved in our section. The subsequent period of decline is
271 interrupted by a second peak in export production which occurred around 65.2 Ma (615.1 mbsf), after
272 which export production flattens out. The initial ~1 Myr period of high, generally declining productivity
273 is also evident in the foraminifera. Benthic foraminifera, dependent on the flux of organic matter from
274 above, are abundant overall in the lower Danian, as are non-spinose, non-symbiont bearing planktic

275 foraminifera, which are best suited to eutrophic environments. The rest of the study interval is
276 characterized by low and stable Ba/Ti ratios (with several small short-lived increases), higher abundances
277 of oligotrophic planktic foraminifera, fewer benthic foraminifera, and an increasingly diverse calcareous
278 nannoplankton assemblage.

279 **3.3 Water Column Structure**

280 Planktic foraminiferal paleoecology also provides insight into local hydrography. Planktic
281 foraminifera occupy specific depth habitats in open ocean environments which can be determined via
282 single-species isotopic analysis (e.g., Aze et al., 2011; Birch et al., 2012). The pervasive foraminiferal
283 recrystallization throughout Site M0077 prevents this kind of geochemical analysis, but fortunately we
284 can use the Paleocene compilation of Aze et al. (2011) to assign the species to depth habitats (Table 2).
285 Here, we use the relative proportion of mixed layer, thermocline, and sub thermocline taxa to reconstruct
286 the degree to which the water column was stratified. Dominance of mixed layer taxa indicates the lack of
287 suitable habitat for thermocline/subthermocline species, suggesting weak stratification with the mixed
288 layer habitat extending through much of the photic zone. Higher abundances of thermocline and
289 subthermocline taxa indicate a more stable habitat for these species, which may result from stronger water
290 column stratification. Conversely, a dominance of mixed layer taxa may indicate the presence of an
291 oxygen minimum zone below the mixed layer preventing colonization of those depths except during
292 particular seasons.

293 Overall, Site M0077 is dominated by mixed layer taxa for the first ~ 200 kyr of the Danian,
294 followed by a shift to more stratified waters from ~ 200-400 kyr (616.3-615.9 mbsf) after the boundary, a
295 return to mixed-layer dominated waters from 400-900 kyr (615.9-614.9 mbsf) after the boundary, and
296 finally a permanent shift toward stable stratified waters after 900 kyr (above 614.9 mbsf).

297 **4. Evolution of surface ocean circulation in the early Chicxulub Crater**

298 Synthesizing this diverse dataset, we interpret a progression from a high productivity, well-mixed
299 water column to one that is oligotrophic and stratified. This progression occurs in several steps (see
300 numbered, shaded bars on Figure 5) as follows:

301 **4.1 High export productivity, well-mixed water column (66.0-65.9 Ma).**

302 The first 100 kyr after the Chicxulub impact (616.5-616.4 mbsf) is characterized by high export
303 production and is dominated by mixed-layer planktic foraminifera, predominantly *Guembelitra*,
304 *Globoconusa*, and *Parvularugoglobigerina*, while the disaster taxon *Cervisiella* dominated the
305 nannoplankton community. Several acmes of planktic foraminifera occurred across the Tethys and North
306 Atlantic after that K-Pg boundary, termed Planktic Foraminiferal Acme Stages (PFAS; Arenillas et al.,
307 2000, 2006, 2016; Alegret et al., 2004). These represent a coeval succession of dominant taxa in open
308 marine sections over a wide geographic area. The presence of these acme stages within the crater (Figure
309 6) is another indication that the planktic foraminiferal populations are representative of at least regional
310 trends and not local processes unique to the crater. PFAS-1, the predominance of *Guembelitra*,
311 corresponds to this earliest interval of post-impact sedimentary rocks.

312 **4.2 High export productivity, increasing stratification (65.9-65.7 Ma).**

313 During the period from 100-300 kyr after the impact (616.4-616.1 mbsf), high export productivity
314 continued but thermocline and sub-thermocline dwelling foraminifera (*Eoglobigerina* and
315 *Chiloguembelina*) become more common. This transition is coincident with a small increase in
316 terrigenous flux (see also Figure 3) which we propose led to the increased stratification. PFAS-2, the
317 predominance of *Globoconusa* and *Parvularugoglobigerina*, occurs in this interval (Figure 6).

318 **4.3 Declining export productivity, well stratified water column (65.7-65.6 Ma).**

319 A sharp drop in export productivity occurred 300 kyr after the boundary (616.1 mbsf) during a
320 period of well-developed water column stratification (indicated both by planktic foraminifer assemblages
321 and the first measurable organic carbon). *Braarudosphaera* became predominant in the nannofossil

322 assemblage, although foraminifer-sized calcispheres (tentatively identified as *Cervisiella*) also bloomed at
323 that this time, suggesting that this taxon may have just become larger. This event is not associated with
324 any evidence for increased terrigenous flux. PFAS-3, the predominance of *Woodringina* and the sub-
325 thermocline-dwelling *Chiloguembelina*, also begins in this interval. This correlation suggests that the
326 changes in stratification observed at Site M0077 are part of larger trends that extend at least across the
327 North Atlantic. The observed stratification may have been driven primarily by the warming that occurred
328 at this time, associated with the Dan-C2 hyperthermal, which is not recorded in our carbon isotope data
329 but occurred at 65.7 Ma (Quillévéré et al., 2008). The lack of the diagnostic isotope excursion for this
330 event here is likely due to a combination of low sedimentation rate and pervasive bioturbation combined
331 with diagenetic alteration of the carbonate; there is no stratigraphic evidence for a hiatus at this level, and
332 no change in sedimentation rate to indicate the absence of ~ 200 kyr worth of sediment.

333 A clear change in export productivity and/or upper water column stratification occurs 300 kyr
334 after the K-Pg boundary at many sites around the globe. In the western Gulf of Mexico, benthic
335 foraminiferal assemblages indicate a return to pre-extinction levels of export production ~300 kyr post
336 impact (Alegret et al., 2001; Alegret and Thomas, 2005), presumably also as a result of the observed
337 regional changes in stratification. Benthic foraminifer assemblages also recover ~300 kyr after the K-Pg
338 boundary on the eastern side of the Atlantic Ocean in Spain (Alegret and Thomas, 2005). PFAS-3 begins
339 around this level, and is characterized in part by a proliferation of *Chiloguembelina* (Arenillas et al.,
340 2000), a sub-thermocline dweller (D'Hondt and Zachos, 1993) also suggesting increased stratification. At
341 the Gubbio section in Italy, the Dan-C2 hyperthermal is also associated with increased stratification as
342 well as an increase in benthic foraminifer abundance, suggesting higher export productivity or a more
343 efficient biological pump (Coccioni et al., 2010). At Walvis Ridge in the South Atlantic, Foraminifer
344 isotope data also indicate an increase in thermal stratification (Birch et al., 2016). At Maud Rise in the
345 Southern Ocean, low Ba/Ti and Ba/Fe ratios begin to recover ~300 kyr after the K-Pg boundary (Hull and
346 Norris, 2011). At Shatsky Rise in the equatorial Pacific, high post-extinction export productivity spikes

347 and then declines ~300 kyr post impact (Hull and Norris, 2011). These sites are broadly distributed
348 geographically, and represent a range of depositional environments. Although there are other sites at
349 which no change is observed at this point in time (e.g., Vigo Seamount, São Paulo Plateau, and Wombat
350 Plateau; Hull and Norris, 2011), we note that the lack of a globally consistent shift in productivity may be
351 considered analogous to the productivity response to the Paleocene-Eocene Thermal Maximum (PETM),
352 which was dominated by local signals (e.g., Gibbs et al., 2006).

353 The widespread, global changes in export production 300 kyr after the K-Pg mass extinction
354 occurred at least 100 kyr before the final cessation of Deccan volcanism (Schoene et al., 2019; Sprain et
355 al., 2019), but it is coeval with the Dan-C2 hyperthermal, suggesting a causal link with this hyperthermal
356 and a lack of evidence for any purported cooling effect from the Deccan volcanism (e.g., Fendley et al.,
357 2019). Unfortunately, the Dan-C2 event has seen relatively little study, and its global effects are poorly
358 understood (e.g., Quillévéré et al., 2008 and Coccioni et al., 2010). Although not as well studied as the
359 Eocene hyperthermals, the Dan-C2 event occurs at a critical moment in Earth's history, as the early K-Pg
360 recovery interval came to an end and new Paleocene organisms became established; we suggest that the
361 Dan-C2 hyperthermal event requires additional focused study.

362 **4.4 Moderate export productivity, poorly stratified water column (65.6-65.2 Ma).**

363 400 kyr after the impact (615.9 mbsf), water column stratification weakened and mixed layer taxa
364 again dominated the assemblage. Benthic foraminifera reached their peak abundance, indicating a well-
365 oxygenated seafloor with an adequate food supply. Foraminifer-sized calcispheres peaked and then
366 declined as *Cerviseilla* again dominated the nannofossil assemblage. Microperforate planktic
367 foraminifera, best adapted to eutrophic conditions, still dominated the foraminiferal population, as did
368 eutrophic nannoplankton taxa (i.e., *Cerviseilla* and *Braarudosphaera*). Taken together, the productivity
369 proxies suggest that surface waters were still eutrophic but that export productivity was declining.

370 **4.5 Stratification redevelops and productivity declines (65.2-64.3 Ma)**

371 Over the next ~ million years (615.2-613.2 mbsf) stratification strengthened, indicated by both
372 planktic foraminifera and TOC, while export productivity slowly declined. Total organic carbon is
373 essentially zero for the first million years of the Danian and is higher, although still low, from 65.0-62.5
374 Ma (Figure 5). TOC enrichment is controlled by both productivity and preservation (e.g., Pederson and
375 Calvert, 1990), so an increase in TOC concurrent with a reduction in export productivity suggests an
376 increase in the preservation potential of organic matter. The most likely mechanism for this increase is
377 reduced ventilation of the seafloor, indicating enhanced stratification at the study area after 65.0 Ma.
378 Increased TOC and decreased export productivity were concurrent with increasing terrigenous flux
379 (Figure 5). Stratification appears to have been linked to increased terrigenous flux, indicated by
380 comparatively elevated Fe, Ti/Al, and magnetic susceptibility through this interval (Figure 3).

381 Declining export productivity was associated with the decline of nannoplankton disaster taxa and
382 the onset of successive acmes of new taxa (“boom-bust successions,” Jones et al., 2019) and an increase
383 in spinose foraminifera, which have a wider diet than non-spinose, non-symbiont-bearing planktics and
384 thus were (and still are) better suited for lower nutrient waters. Jones et al. (2019) suggested that declining
385 productivity was due to the local recovery of the biological pump; our data indicate that this increased
386 pump efficiency was tied to an increase in stratification. Stratification limits the upwelling of deeper,
387 more nutrient rich waters. Nutrient poor waters are, perhaps counter-intuitively, characterized by a more
388 efficient biological pump than eutrophic waters, as a higher proportion of nutrients are exported out of the
389 photic zone (e.g., Hilting et al., 2008). At Site M0077, this change in photic zone nutrient concentrations
390 disturbed the stable eutrophic disaster nannoplankton assemblage and began a succession of acmes of taxa
391 better adapted to lower nutrient conditions (Figure 6; Jones et al., 2019).

392 **4.6 Stable, Stratified Water Column (64.3-63.5 Ma)**

393 The rest of the lower Paleocene record at Site M0077 (613.2-611.6 mbsf), below a series of
394 stacked unconformities spanning the uppermost Danian to the PETM, documents a stable, stratified,
395 oligotrophic, open-ocean environment. Following the *Praeprinsius* nannoplankton acme, which

396 terminates around 63.4 Ma (Jones et al., 2019), the post-extinction ecosystem was finally stabilized. The
397 lead-up to the Latest Danian Event (LDE – just above the study interval) was also characterized by a well-
398 stratified upper water column at Shatsky Rise in the Pacific Ocean (Jehle et al., 2015). Our results show
399 that in the Gulf of Mexico, at least, increased stratification predates the LDE by several million years.

400 **4.7 Controls on Stratification**

401 The Chicxulub basin was open to the northeast (Gulick et al., 2008) and thus well connected to
402 the rest of the Gulf of Mexico through the entire depth of the crater. The observed changes in
403 stratification (Figure 3) are not, then, the result of restriction in a silled basin. The first major change in
404 stratification, about 65.8 Ma (~616.3 mbsf), is coincident with a small rise in terrigenous flux, likely
405 associated with increased freshwater input into the Gulf of Mexico basin. The elevated terrigenous input
406 declines but the stratification persists during the period of the Dan-C2 hyperthermal event (Quillévére et
407 al., 2008); the hyperthermal event and local stratification both end around 65.5 Ma (~615.7 mbsf). The re-
408 establishment of a large sub-thermocline population coincides with a second, larger, longer pulse of
409 enhanced weathering that occurred between 65.0 and 65.3 Ma (~615.2-615.0 mbsf), toward the end of the
410 decline in export productivity. The interval of a well-stratified water column after 65.0 Ma (~615.0 mbsf)
411 corresponds to higher background rates of terrigenous flux, and we conclude that changing rates of
412 freshwater input into the

413 **4.8 Global Context**

414 The earliest Danian oceanic environment is often referred to as “unstable” (e.g., Hull et al., 2011).
415 Our data suggest at least one component of this instability is a fluctuating degree of water column
416 stratification, which in turn appears related to changes in export productivity and pelagic ecosystem
417 structure. Overall, stratification appears anti-correlated with export productivity. We conclude that the
418 degree of stratification is a likely driver for the observed trends in export productivity. A well-mixed
419 water column could sustain enhanced primary productivity by delivering nutrients to the photic zone,

420 while a stratified water column limits such mixing. Increased biological pump efficiency at lower nutrient
421 levels (e.g., Hiltung et al., 2008) facilitated increased oligotrophy once stratification caused an initial
422 decline in photic zone nutrient content. An increase in stratification, driven by an increase in freshwater
423 flux into the Gulf of Mexico, could thus lead to the observed shift from eutrophic to oligotrophic waters.

424 Strengthening stratification corresponds to the decline in the dominance of *Cervisiella* ~ 200 kyr
425 after the boundary and immediately precedes the beginning of boom-bust successions of calcareous
426 nannoplankton (Jones et al., 2019) ~1 Myr after the K-Pg boundary. We propose that stratification-
427 moderated changes in nutrient content were the ultimate control on the anomalously long delay in the
428 recovery of species diversity in calcareous nannoplankton at ground zero (Jones et al., 2019). Global
429 changes in stratification around 300 kyr after the boundary, possibly related to the Dan-C2 hyperthermal,
430 provide an explanation for observed changes in export production that occurred at that time.

431 **4. Conclusions**

432 High export productivity in the Chicxulub crater decreased sharply ~300 kyr after the K-Pg
433 boundary at 66 Ma, slowly declined for another 700 kyr, and then remained low through the next ~ 1
434 Myr, through ~63 Ma. The record of increased stratification and decreased export production at Site
435 M0077, concurrent with an increase in biological pump efficiency, are the likely cause of the observed
436 decline of the post-impact nannoplankton disaster assemblages and the diversification characterized by
437 successive blooms of Paleocene taxa (Jones et al., 2019). A shift in export production around 300 kyr into
438 the Danian is a feature of many records across the oceans and indicates that the trends in export
439 productivity at Site M0077 are not unique to the crater. Instead, declining productivity appears to be
440 initiated by increased stratification in the Gulf of Mexico, caused both by warming during the Dan-C2
441 hyperthermal and by a general increase of freshwater input into the Gulf, and sustained by increases in
442 biological pump efficiency. The sharp decline in export production during the Dan-C2 coincides with
443 changes in productivity and stratification at many sites across the world, and we believe that this indicates
444 that a global increase in stratification disturbed recovery ecosystems, spurred a recovery of the biological

445 pump, and drove a turnover in the plankton.

446 **Data Availability Statement**

447 Planktic foraminifer data and XRF core scan data will be uploaded to the NOAA National Climate Data
448 Center before publication. Calcareous nannoplankton data are from Jones et al. (2019) and are archived as
449 [GSA Data Repository Item 2019271](#).

450

451 **Acknowledgements**

452 The authors acknowledge NSF OCE 1737351. We are grateful to Pincelli Hull for her helpful discussions
453 on our data and hers, and to the staff of the Bremen Core Repository for their invaluable help sampling and
454 scanning the core. We also thank Tessa Cayton for her assistance preparing foraminifer samples. I.A. and
455 J.A.A. acknowledge the use of the Servicio General de Apoyo a la Investigación-SAI, Universidad de
456 Zaragoza. The European Consortium for Ocean Research Drilling (ECORD) implemented Expedition 364
457 with funding from the International Ocean Discovery Program (IODP) and the International Continental
458 scientific Drilling Project (ICDP). Data and samples can be requested from IODP. U.S. participants in Exp.
459 364 were supported by the U.S. Science Support Program. J.V.M. was funded by NERC, Grant:
460 NE/P005217/1. I.A. and J.A.A. were supported by MINECO/FEDER-UE (project number CGL2015-
461 64422-P) and MCIU/AEI/FEDER, UE (project number PGC2018-093890-B-I00). This is UTIG
462 Contribution #XXXX.

463

464 **Appendix 1**

465 **Expedition 364 Science Party:** Elise Chenot, Gail Christeson, Philippe Claeys, Charles
466 Cockell, Marco J. L. Coolen, Ludovic Ferrière, Catalina Gebhardt, Kazuhisa Goto, Sophie
467 Green, Sean Gulick, Heather Jones, David A. Kring, Johanna Lofi, Christopher M. Lowery,
468 Claire Mellett, Joanna Morgan, Rubén Ocampo-Torres, Ligia Perez-Cruz, Annemarie
469 Pickersgill, Michael Poelchau, Auriol Rae, Cornelia Rasmussen, Mario Rebolledo-Vieyra, Ulrich

470 Riller, Honami Sato, Jan Smit, Sonia Tikoo, Naotaka Tomioka, Jaime Urrutia-Fucugauchi,
471 Michael Whalen, Axel Wittmann, Long Xiao, Kosei Yamaguchi, William Zylberman

472

473

474

475

476

477

478

479

480

481

482

483

484

485

486

487

488

489

490 **Table 1.** Biostratigraphic datums for the Paleocene interval of Hole M0077A. Nannofossil datums
 491 marked with asterisks are not used in the age model. Datum ages after Gradstein et al. (2012).

Taxon	Zone	Sample Above	Sample Below	Avg. Depth	Datum Age
<i>Discoaster multiradiatus</i>	Base of CP8	607.26	607.37	607.315	57.21
<i>Morozovella acuta</i>	Base of P4b	607.52	607.76	607.65	57.79
<i>Heliolithus kleinpellii</i> *	Base of CP5	607.52	607.76	607.65	59.94
<i>Igorina pusilla</i>	Base of P3a	609.28	609.3	609.29	62.6
<i>Praemurica uncinata</i>	Base of P2	610.6	610.65	610.63	63
<i>Globanomalina compressa</i>	Base of P1c	612.36	612.41	612.385	63.9
<i>Chiasmolithus danicus</i> *	Base of CP2	612.5	612.75	612.625	64.81
<i>Subbotina triloculinoidea</i>	Base of P1b	615.21	615.26	615.235	65.25
<i>Parvularugoglobigerina eugubina</i>	Base of P1a	616.15	616.2	616.175	65.72
<i>Parvularugoglobigerina eugubina</i>	Base P α	616.56	616.56	616.56	66

492

493 **Table 2.** Planktic foraminifer depth habitat assignments based on the ecogroups of Aze et al., 2011. All assignments are from that paper unless
 494 otherwise noted. No taxa assigned to Groups 5 and 6 appear in our dataset.

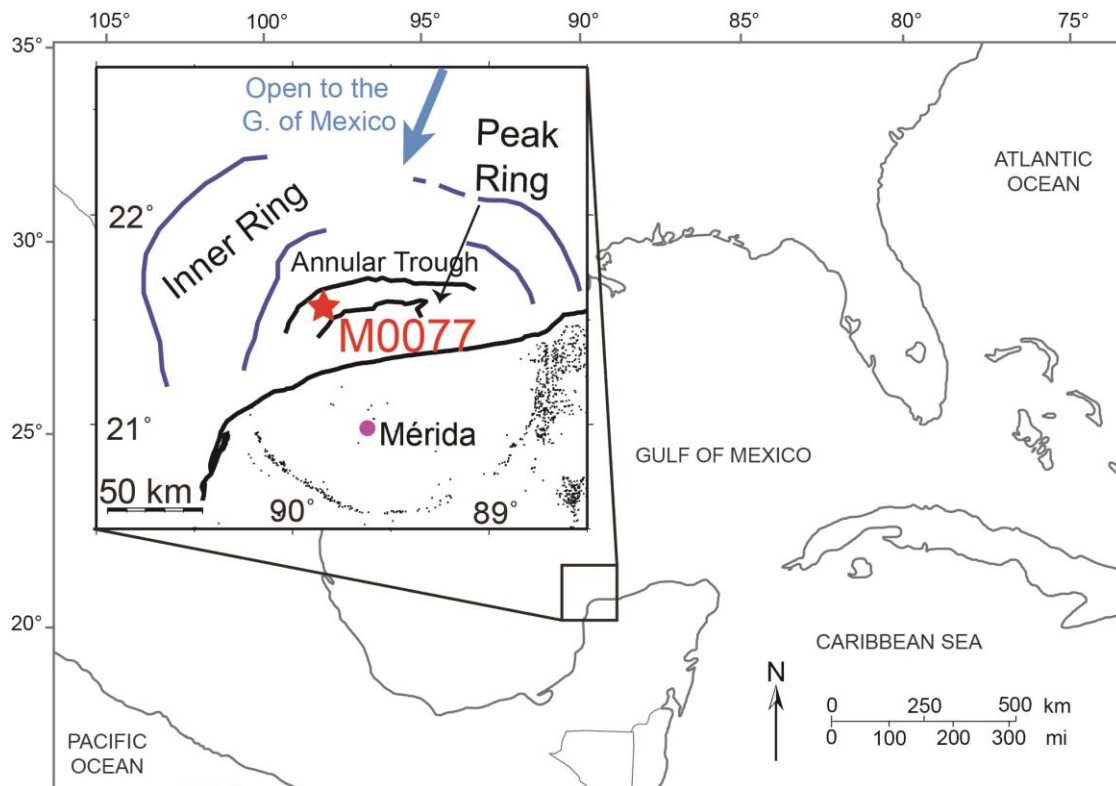
Aze et al. 2011 ecogroups	Group	Explanation	Members
Group 1	Open ocean mixed-layer tropical/subtropical, with symbionts	Very heavy $\delta^{13}\text{C}$ and relatively light $\delta^{18}\text{O}$	<i>Morozovella</i> , <i>Igorina</i> , <i>Acarinina</i> , <i>Praemurica inconstans</i> ~,
Group 2	Open Ocean mixed-layer tropical/subtropical, without symbionts	$\delta^{13}\text{C}$ lighter than species with symbionts; also relatively light $\delta^{18}\text{O}$	<i>Guembelitra</i> *, <i>Parvularugoglobigerina</i> *, <i>Woodringina</i> *, <i>Globoconusa daubjergensis</i> *†, <i>Rectuvigerina cretacea</i> *, <i>Praemurica taurica</i> , <i>Praemurica pseudoinconstans</i> , <i>Subbotina triangularis</i> , <i>Praemurica uncinata</i>
Group 3	Open Ocean thermocline	Light $\delta^{13}\text{C}$ and relatively heavy $\delta^{18}\text{O}$	<i>Globanomalina</i> , <i>Eoglobogerina</i> <i>Parasubbotina varianta</i> , <i>Subbotina trivialis</i> , <i>Subbotina triloculinoides</i>
Group 4	Open Ocean sub-thermocline	Very light $\delta^{13}\text{C}$ and very heavy $\delta^{18}\text{O}$	<i>Chiloguembelina midwayensis</i> *, <i>Chiloguembelina morsei</i> ^, <i>P. pseudobulloides</i>
Group 5	High Latitude	Species only found in high latitude sites	N/A
Group 6	Upwelling/high productivity	Species only found in sites of high productivity or upwelling	N/A

*Olsson et al., 1999 and references therein

†Olsson (1999): "Although its abundance in near-shore sequences indicates a near-surface planktic habitat (Troelsen, 1957; Keller, 1989; Liu and Olsson, 1992), its oxygen isotopic signature and open-marine abundance patterns suggest a preference for relatively cool water masses (Premoli Silva and Boersma, 1989; D'Hondt and Keller, 1991; Liu and Olsson, 1992; D'Hondt and Zachos, 1993)."

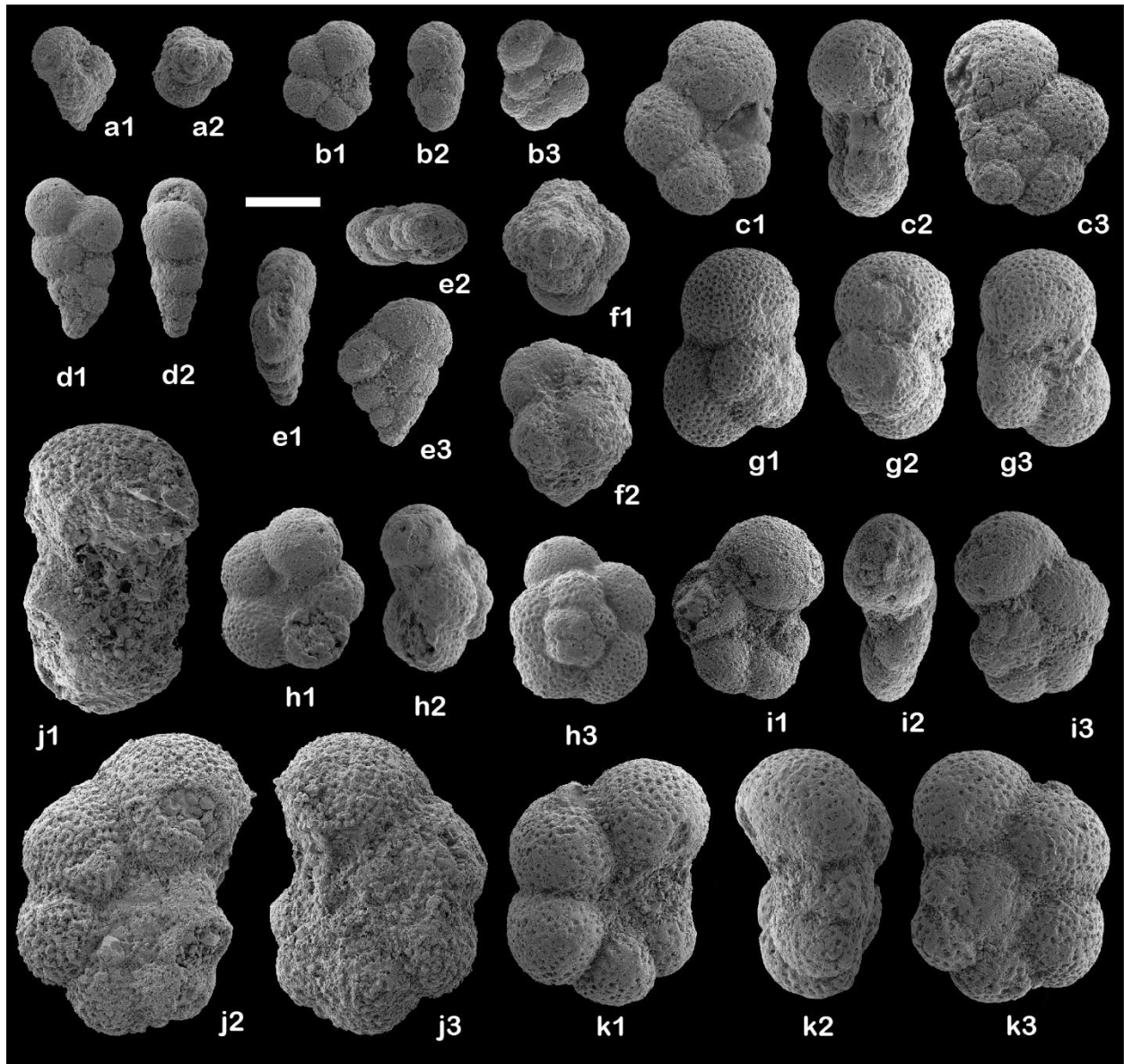
~Norris (1996) and Birch et al. (2012) describe *P. inconstans* as first symbiont-bearing planktic.

^no isotope data are available for any other Paleocene Chiloguembelinids, so we place *Ch. morsei* in this group based on the data from its cousin *Ch. midwayensis*.



496

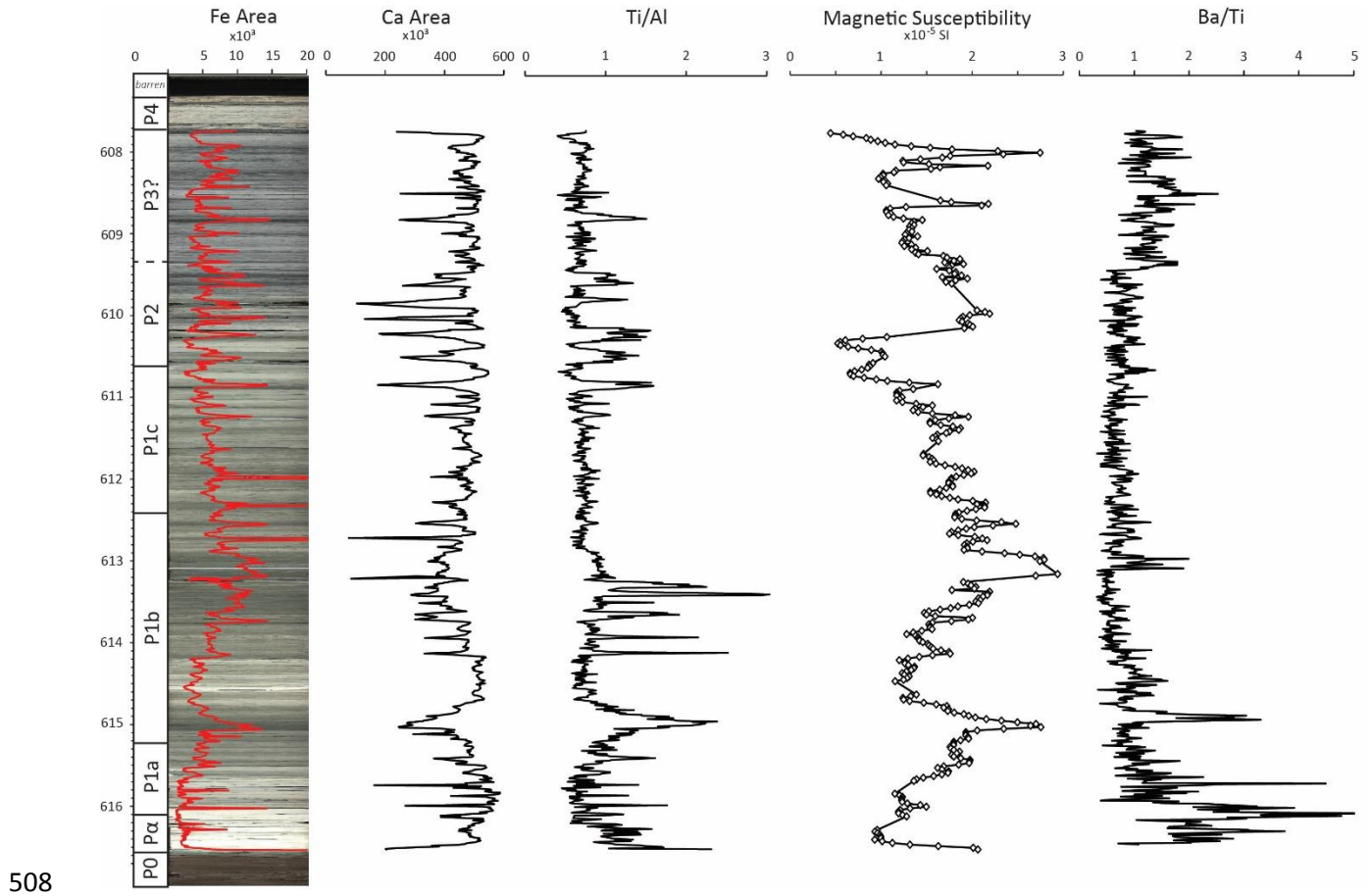
497 **Figure 1.** Location map showing the position of IODP Site M0077 within the Chicxulub crater.



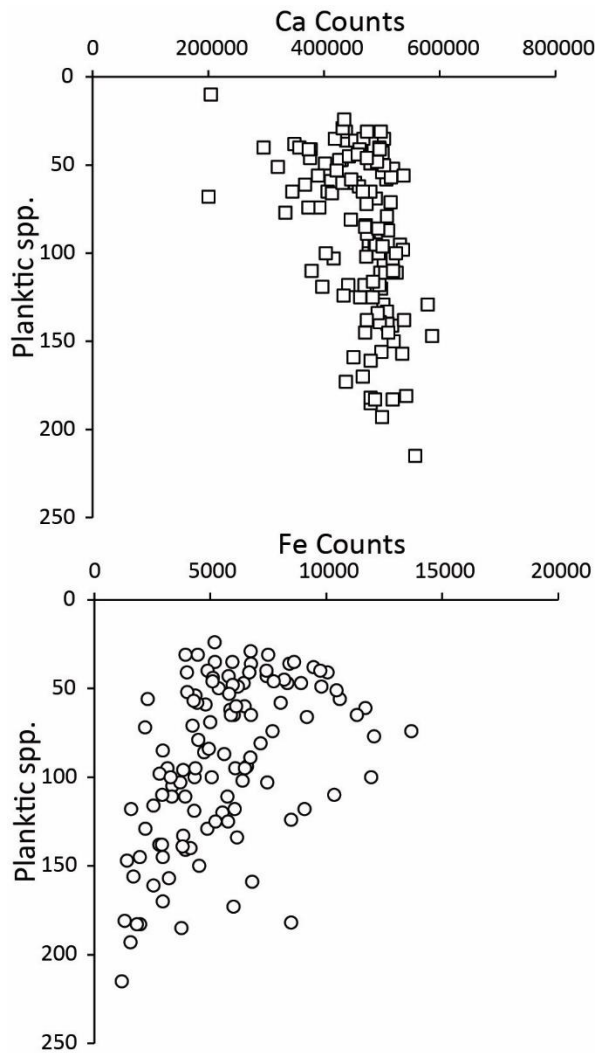
498

499 **Figure 2.** SEM images of planktic foraminiferal index-species and other relevant species (scale bar = 100
 500 microns). (a) *Guembelitra cretacea* (364-M0077A-39R-2 85-86 cm); (b) *Parvularugoglobigerina*
 501 *eugubina* (364-M0077A-40R-1 17-18 cm); (c) *Parasubbotina pseudobulloides* (364-M0077A-39R-1 128-
 502 129 cm); (d) *Chiloguembelina morsei* (364-M0077A-39R-2 98-99 cm); (e) *Chiloguembelina*
 503 *midwayensis* (364-M0077A-39R-3 41-42 cm); (f) *Globoconusa daubjergensis* (364-M0077A-37R-2 116-
 504 117 cm); (g) *Subbotina triloculinoides* (364-M0077A-38R-2 60-61 cm); (h) *Eoglobigerina edita* (364-
 505 M0077A-38R-2 60-61 cm); (i) *Globanomalina compressa* (364-M0077A-37R-1 116-117 cm);

506 (j) *Praemurica uncinata* (364-M077A-37R-1 96-97 cm); (k) *Praemurica inconstans* (364-M0077A-37R-2
507 37-38 cm).

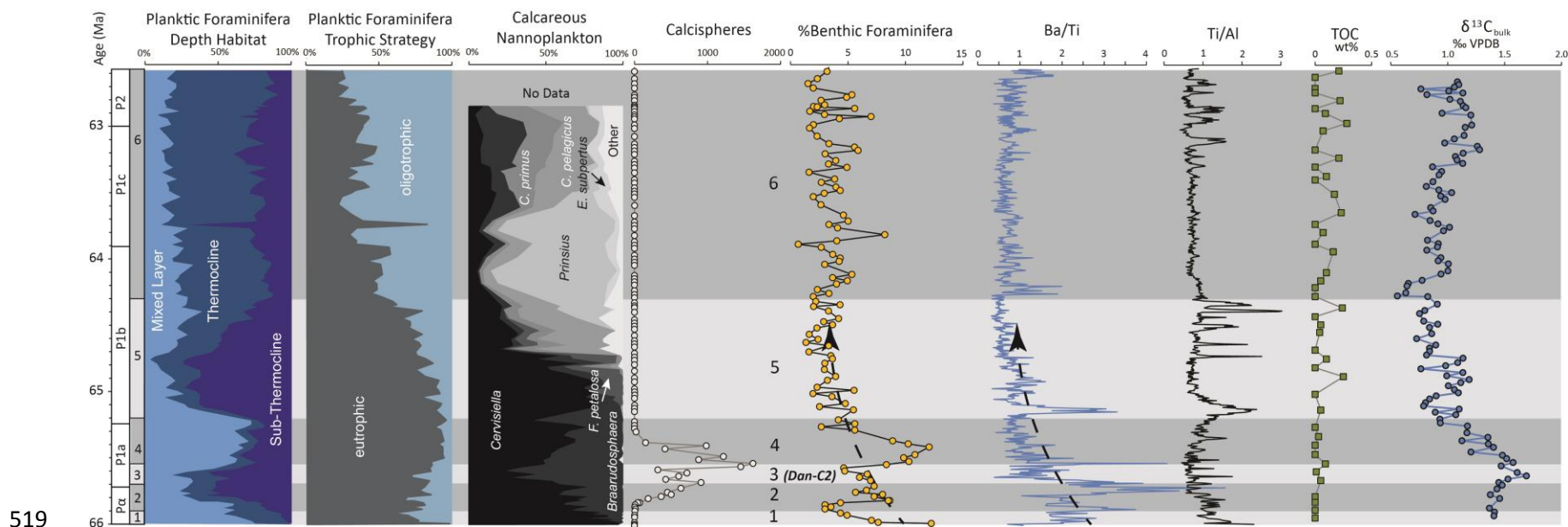


509 **Figure 3.** Sedimentological proxies vs. depth. Core linescan composite of the Paleocene interval at Site
510 M0077 is overlaid by XRF Fe counts. Increased Fe, decreased Ca, increased Ti/Al, and higher magnetic
511 susceptibility are all proxies for higher terrigenous flux. Increased Ba/Ti indicated higher local export
512 productivity.

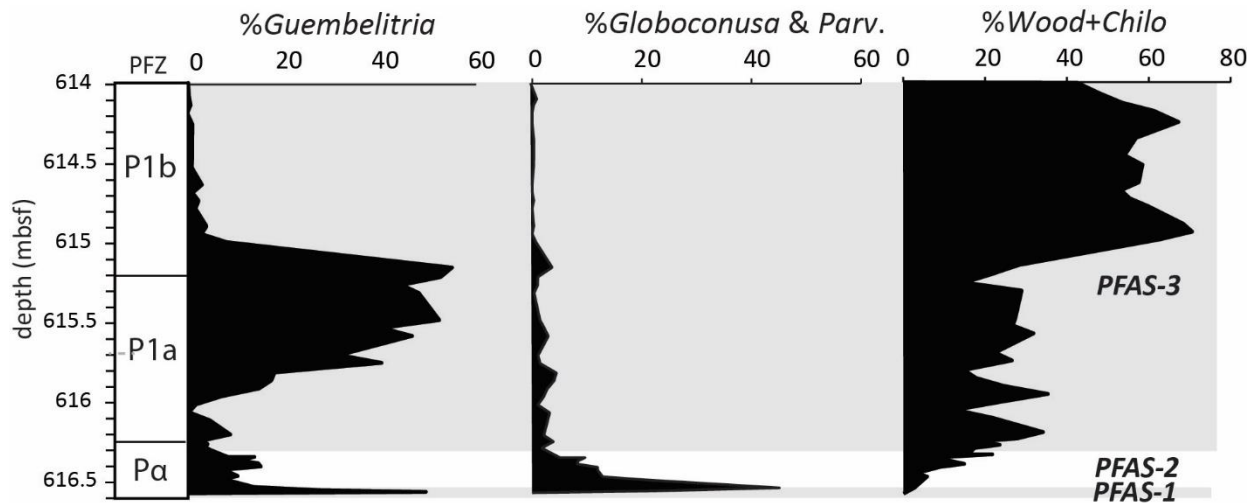


513

514 **Figure 4.** Preservation vs Calcium and Iron XRF counts. Better preservation is toward zero on the y-axis
 515 (i.e., fewer unidentifiable foraminifera). Two outliers >80,000 from pyrite-rich samples at the base of the
 516 section were removed from the Fe plot. Ca shows a weak negative correlation with good preservation while
 517 Fe shows a weak positive correlation with good preservation. This pattern is the opposite of what would be
 518 expected if these trends were caused by dissolution.



520 **Figure 5.** Paleoclimatology proxies plotted by age. Planktic foraminifer by depth habitat record the stratification of the upper water column; see
 521 Table 2 for species assigned to mixed layer, thermocline, and subthermocline planktic foraminifer groups. Planktic foraminifera by trophic strategy
 522 record changes in paleoproductivity, Calcareous nannoplankton diversity shows the relative abundance of all (non-reworked) species of calcareous
 523 nannoplankton present. Calcispheres shows the abundance of calcispheres >45 μm. %Benthics is the percentage of benthic foraminifera relative to
 524 all foraminifera, and probably responds primarily to nutrient flux to the seafloor. Ba/Ti records paleoproductivity, with high ratios indicating high
 525 productivity. Ti/Al records terrigenous flux (see Fig. 4) and TOC (total organic carbon) corresponds to changes in preservation potential at the
 526 seafloor; here, preservation increase is probably due to water column stratification.



528 **Figure 6.** Quantitative stratigraphic distribution of early Danian planktic foraminiferal groups at Site
 529 M0077 and Planktic Foraminiferal Acme Stages (PFAS) 1-3: PFAS-1 is the predominance of *Guembelitra*,
 530 PFAS-2 is the predominance of *Parvularugoglobigerina* and *Globoconusa* (or *Palaeoglobigerina*
 531 according to Arenillas and Arz, 2017), and PFAS-3 is the predominance of *Woodringina* and
 532 *Chiloguembelina*. A second acme of *Guembelitra* (or *Chiloguembelitra* according to Arenillas and Arz,
 533 2017) occurs within this stage across the Tethys, as is also evident at Site M0077.

534

535

536

537

538

539

540

541

542 **REFERENCES**

- 543 Alegret, L., Molina, E., & Thomas, E. (2001). Benthic foraminifera at the Cretaceous-Tertiary boundary
544 around the Gulf of Mexico. *Geology*, 29, 891-894.
- 545 Alegret, L., & Thomas, E. (2005). Cretaceous/Paleogene boundary bathyal paleo-environments in the
546 central North Pacific (DSDP Site 465), the Northwestern Atlantic (ODP Site 1049), the Gulf of
547 Mexico and the Tethys: The benthic foraminiferal record. *Palaeogeography, Palaeoclimatology,*
548 *Palaeoecology*, 224, 53-82.
- 549 Alegret, L., Arenillas, I., Arz, J. A., & Molina, E. (2004). Foraminiferal event-stratigraphy across the
550 Cretaceous/Paleogene boundary. *Neues Jahrbuch für Geologie und Paläontologie - Abhandlungen*,
551 234, 25-50.
- 552 Alegret, L., E. Thomas, & K.C. Lohmann (2012), End-Cretaceous marine mass extinction not caused by
553 productivity collapse, *Proceedings of the National Academy of Sciences*, 109(3), 728-732.
- 554 Alvarez, L.W., Alvarez, W., Asaro, F., & Michel, H.V., 1980. Extraterrestrial cause of the Cretaceous–
555 Tertiary extinction. *Science* 208, 1095–1108.
- 556 Arenillas, I., Arz, J. A., Molina, E., & Dupuis, C. (2000). An independent test of planktic foraminiferal
557 turnover across the Cretaceous/Paleogene (K/P) boundary at El Kef, Tunisia; catastrophic mass
558 extinction and possible survivorship. *Micropaleontology*, 46, 31-49.
- 559 Arenillas, I., Arz, J.A., Grajales-Nishimura, J.M., Murillo-Muñetón, G., Alvarez, W., Camargo-Zanoguera,
560 A., Molina, E., Rosales-Domínguez, C. (2006). Chicxulub impact event is Cretaceous/Paleogene
561 boundary in age: new micropaleontological evidence. *Earth and Planetary Science Letters*, 249,
562 241-257.

563 Arenillas, I., Arz, J.A., Grajales-Nishimura, J.M., Rojas-Consuegra, R. (2016). The Chicxulub impact is
564 synchronous with the planktonic foraminifera mass extinction at the Cretaceous/Paleogene
565 boundary: new evidence from the Moncada section, Cuba. *Geologica Acta*, 14(1), 35-51.

566 Arenillas, I., Arz, J.A. (2017). Benthic origin and earliest evolution of the first planktonic foraminifera after
567 the Cretaceous/Paleogene boundary mass extinction. *Historical Biology*, 29, 17-24.

568 Artemieva N. et al., 2017, Quantifying the Release of Climate-Active Gases by Large Meteorite Impacts
569 With a Case Study of Chicxulub, *Geophysical Research Letters*, ISSN: 0094-8276

570 Aze, T., Ezard, T.H.G., Purvis, A., Coxall, H.K., Stewart, D.R.M., Wade, B.S., & Pearson, P.N. (2011), A
571 phylogeny of Cenozoic macroperforate planktonic foraminifera from fossil data, *Biological*
572 *Reviews*, 86, 900-927.

573 Bains, S., Norris, R.D., Corfield, R.M., & Faul, K.L. (2000). Termination of global warmth at the
574 Palaeocene/Eocene boundary through productivity feedback. *Nature*, 407, 171.

575 Bardeen, C. G., Garcia, R. R., Toon, O. B., & Conley, A. J. (2017). On transient climate change at the
576 Cretaceous– Paleogene boundary due to atmospheric soot injections. *Proceedings of the National*
577 *Academy of Sciences*, 114(36), E7415-E7424.

578 Berggren, W. A., & Pearson, P. N. (2005). A revised tropical to subtropical Paleogene planktonic
579 foraminiferal zonation. *The Journal of Foraminiferal Research*, 35, 279-298.

580 Birch, H. S., Coxall, H. K., & Pearson, P. N. (2012). Evolutionary ecology of Early Paleocene planktonic
581 foraminifera: size, depth habitat and symbiosis. *Paleobiology*, 38(3), 374-390.

582 Birch, H.S., Coxall, H.K., Pearson, P.N., Kroon, D., & Schmidt, D.N. (2016). Partial collapse of the
583 marine carbon pump after the Cretaceous-Paleogene boundary. *Geology*, 44, 287-290.

584 Boersma, A., & Silva, I.P. (1989). Atlantic Paleogene biserial heterohelcid foraminifera and oxygen
585 minima. *Paleoceanography*, 4, 271-286.

586 Bown, P. (1998). *Calcareous nannofossil biostratigraphy* (pp. 1-315). Chapman and Hall; Kluwer
587 Academic.

588 Bralower, T.J., Silva, I.P. & Malone, M.J., 2002. New evidence for abrupt climate change in the Cretaceous
589 and Paleogene: An Ocean Drilling Program expedition to Shatsky Rise, northwest Pacific. *GSA*
590 *TODAY*, 12, pp.4-10.

591 Brugger, J., Feulner, G., & Petri, S. (2017). Baby, it's cold outside: Climate model simulations of the
592 effects of the asteroid impact at the end of the Cretaceous. *Geophysical Research Letters*, 44,
593 419-427.

594 Coccioni, R., Frontalini, F., Bancalà, G., Fornaciari, E., Jovane, L., & Sprovieri, M. (2010). The Dan-C2
595 hyperthermal event at Gubbio (Italy): Global implications, environmental effects, and
596 cause(s). *Earth and Planetary Science Letters*, 297, 298-305.

597 Collins, G.S., Patel, N., Rae, A.S., Davies, T.M., Morgan, J.V. Gulick, S.P.S. and Expedition 364
598 Scientists (2017). Numerical simulations of Chicxulub crater formation by oblique impact. *Lunar*
599 *and Planetary Science Conference XLVII*, abstract #1832.

600 Coxall, H.K., S. D'Hondt, & J.C. Zachos (2006), Pelagic evolution and environmental recovery after the
601 Cretaceous-Paleogene mass extinction, *Geology*, 34(4), 297-300.

602 Culver, S.J. (1988), New foraminiferal depth zonation of the northwestern Gulf of Mexico, *Palaios*, 3,
603 69–85.

604 Culver, S. J. (2003). Benthic foraminifera across the Cretaceous–Tertiary (K–T) boundary: a
605 review. *Marine Micropaleontology*, 47(3-4), 177-226.

606 D'Hondt, S., & Keller, G. (1991). Some patterns of planktic foraminiferal assemblage turnover at the
607 Cretaceous-Tertiary boundary. *Marine Micropaleontology*, 17, 77-118.

- 608 D'Hondt, S., & Zachos, J.C. (1993). On stable isotopic variation and earliest Paleocene planktonic
609 foraminifera. *Paleoceanography*, 8, 527-547.
- 610 D'Hondt, S., King, J., & Gibson, C. (1996). Oscillatory marine response to the Cretaceous-Tertiary
611 impact. *Geology*, 24, 611-614.
- 612 D'Hondt, S., Donaghay, P., Zachos, J.C., Luttenberg, D., & Lindinger, M. (1998). Organic carbon fluxes
613 and ecological recovery from the Cretaceous-Tertiary mass extinction. *Science*, 282, 276-279.
- 614 D'Hondt, S., & Zachos, J.C. (1998). Cretaceous foraminifera and the evolutionary history of planktic
615 photosymbiosis. *Paleobiology*, 24, 512-523.
- 616 Dymond, J., Suess, E., & Lyle, M. (1992). Barium in deep-sea sediment: A geochemical proxy for
617 paleoproductivity, *Paleoceanography*, 7, 163-181. doi:10.1029/92PA00181
- 618 Eagle, M., Paytan, A., Arrigo, K.R., van Dijken, G., & Murray, R.W. (2003). A comparison between excess
619 barium and barite as indicators of carbon export, *Paleoceanography*, 18, 1021.
620 doi:10.1029/2002PA000793
- 621 Edgar, K.M., Wilson, P.A., Sexton, P.F., & Suganuma, Y., (2007) No extreme glaciation during the main
622 Eocene calcite compensation depth shift, *Nature*, 448, 908-911.
- 623 Esmeray-Senlet, S., Wright, J.D., Olsson, R.K., Miller, K.G., Browning, J.V., & Quan, T.M. (2015).
624 Evidence for reduced export productivity following the Cretaceous/Paleogene mass extinction,
625 *Paleoceanography*, 30, doi:10.1002/2014PA002724.
- 626 Fraass, A.J., Kelly, D.C., & Peters, S.E. (2015), Macroevolutionary history of the planktic
627 foraminifera *Annual Reviews of Earth and Planetary Science*, 43, 139-166.
- 628 Francois, R., Honjo, S., Manganini, S.J., & Ravizza, G.E. (1995). Biogenic barium fluxes to the deep sea:
629 Implications for paleoproductivity reconstruction, *Global Biogeochemical Cycles*, 9, 289-303.
630 doi:10.1029/95GB00021.

631 Galloway, W.E., Ganey-Curry, P.E., Li, X., & Buffler, R.T. (2000), Cenozoic depositional history of the
632 Gulf of Mexico basin, *AAPG Bulletin*, 84, 1743-1774.

633 Gertsch, B., Keller, G., Adatte, T., Garg, R., Prasad, V., Berner, Z., & Fleitmann, D. Environmental effects
634 of Deccan volcanism across the Cretaceous–Tertiary transition in Meghalaya, India, *Earth and
635 Planetary Science Letters* **310** 272-285 (2011).

636 Gibbs, S.J., Bralower, T.J., Bown, P.R., Zachos, J.C., & Bybell, L.M. (2006). Shelf and open-ocean
637 calcareous phytoplankton assemblages across the Paleocene-Eocene Thermal Maximum:
638 Implications for global productivity gradients. *Geology*, 34, 233-236.

639 Gooday, A.J., (2003), Benthic Foraminifera (Protista) as tools in deep-water palaeoceanography:
640 environmental influences on faunal characteristics, *Advances in Marine Biology*, 46, 1–90.

641 Gradstein, F.M., Ogg, J.G., Schmitz, M., & Ogg, G., Eds. (2012), *The Geologic Times Scale 2012*.
642 Elsevier B.V., Amsterdam, Netherlands.

643 Griffith, E.M., & Paytan, A. (2012). Barite in the ocean—occurrence, geochemistry and
644 palaeoceanographic applications. *Sedimentology*, 59, 1817-1835.

645 Gulick, S.P., Barton, P.J., Christeson, G.L., Morgan, J.V., McDonald, M., Mendoza-Cervantes, K.,
646 Pearson, Z.F., Surendra, A., Urrutia-Fucugauchi, J., Vermeesch, P.M., & Warner, M.R. (2008).
647 Importance of pre-impact crustal structure for the asymmetry of the Chicxulub impact
648 crater. *Nature Geoscience*, 1, 131.

649 Gulick, S., Morgan, J., Mellett, C.L., Green, S.L., Bralower, T., Chenot, E., Christeson, G., Claeys, P.,
650 Cockell, C., Coolen, M.J.L., Ferrière, L., Gebhardt, C., Goto, K., Jones, H., Kring, D., Lofi, J.,
651 Lowery, C., Ocampo-Torres, R., Perez-Cruz, L., Pickersgill, A.E., Poelchau, M., Rae, A.,
652 Rasmussen, C., Rebolledo-Vieyra, M., Riller, U., Sato, H., Smit, J., Tikoo, S., Tomioka, N.,
653 Urrutia- Fucugauchi, J., Whalen, M., Wittmann, A., Yamaguchi, K., Xiao, L., & Zylberman, W.,

654 2017. Site M0077: Post-Impact Sedimentary Rocks. *In* Morgan, J., Gulick, S., Mellett, C.L.,
655 Green, S.L., and the Expedition 364 Scientists, *Chicxulub: Drilling the K-Pg Impact*
656 *Crater*. Proceedings of the International Ocean Discovery Program, 364: College Station, TX
657 (International Ocean Discovery Program). <https://doi.org/10.14379/iodp.proc.364.105.2017>

658 Gulick, S.P.S., Bralower, T.J., Ormö, J., Hall, B., Grice, K., Schaefer, B., Lyons, S., Freeman, K.H.,
659 Morgan, J.V., Artemieva, N., Kaskes, P., de Graff, S.J., Whalen, M.T., Collins, S.M., Verhagen,
660 C., Christeson, G.L., Claeys, P., Coolen, M.J., Goderis, S., Goto, K., Grieve, R., McCall, N.,
661 Osinski, G.R., Rae, A., Riller, U., Smit, J., Vajda, V., Wittman, A., and Expedition 364 Scientists,
662 *(In Press)* The First Day of the Cenozoic. *Proceedings of the National Academy of Sciences*.

663 Hemleben, C., Spindler, M., & Anderson, O. R. (1989). *Modern planktonic foraminifera*. Springer
664 Science & Business Media.

665 Hemleben, C., Mühlen, D., Olsson, R.K., & Berggren, W.A. (1991). Surface texture and the first
666 occurrence of spines in planktonic foraminifera from the early Tertiary. *Geologisches Jahrbuch*,
667 128, 117-146.

668 Hildebrand, A.R., Penfield, G.T., Kring, D.A., Pilkington, M., Camargo, A.Z., Jacobsen, S.B., & Boynton,
669 W.V., 1991. Chicxulub Crater: a possible Cretaceous/Tertiary boundary impact crater on the
670 Yucatán Peninsula, Mexico. *Geology* 19, 867–871.

671 Hsü, K.J., & McKenzie, J.A. (1985). A “Strangelove” ocean in the earliest Tertiary. *The Carbon Cycle and*
672 *Atmospheric CO: Natural Variations Archean to Present*, 487-492.

673 Hull, P.M., & R.D. Norris (2011), Diverse patterns of ocean export productivity change across the
674 Cretaceous-Paleogene boundary: New insights from biogenic barium, *Paleoceanography*, 26(3).

675 Hull, P. M., Norris, R. D., Bralower, T. J., & Schueth, J. D. (2011). A role for chance in marine recovery
676 from the end-Cretaceous extinction. *Nature Geoscience*, 4, 856-860.

677 Jablonski, D. (1995) in *Extinction Rates* (eds. Lawton, J. H. & May, R. M.) 25–44 Oxford Univ. Press,
678 Oxford.

679 Jehle, S., Bornemann, A., Deprez, A., & Speijer, R.P. (2015). The impact of the latest Danian event on
680 planktic foraminiferal faunas at ODP site 1210 (Shatsky rise, Pacific Ocean). *PloS one*, 10,
681 e0141644.

682 Jiang, S., T.J. Bralower, M.E. Patzkowsky, L.R. Kump, & J.D. Schueth (2010), Geographic controls on
683 nannoplankton extinction across the Cretaceous/Palaeogene boundary, *Nature Geoscience*, 3(4),
684 280.

685 Jones, H., Lowery, C.M., and Bralower, T. (*Accepted*). Delayed calcareous nannoplankton boom-bust
686 successions in the earliest Paleocene Chicxulub Crater. *Geology*.
687 <https://doi.org/10.1130/G46143.1>

688 Jorissen, F.J., H.C. de Stigter, & J.G.V. Widmark, (1995), A conceptual model explaining benthic
689 foraminiferal microhabitats, *Marine Micropaleontology*, 26, 3–15.

690 Keller, G. (1989). Extended Cretaceous/Tertiary boundary extinctions and delayed population change in
691 planktonic foraminifera from Brazos River, Texas. *Paleoceanography and Paleoclimatology*, 4,
692 287-332.

693 Kominz, M.A., Browning, J.V., Miller, K.G., Sugarman, P.J., Mizintseva, S., & Scotese, C.R. (2008).
694 Late Cretaceous to Miocene sea-level estimates from the New Jersey and Delaware coastal plain
695 coreholes: an error analysis. *Basin Research*, 20, 211-226.

696 Knoll, A.H. & Follows, M.J. (2016) A bottom-up perspective on ecosystem change in Mesozoic oceans,
697 *Proceedings of the Royal Society B* 283 2016755.

698 Kring, D. A. (2007). The Chicxulub impact event and its environmental consequences at the Cretaceous–
699 Tertiary boundary: *Palaeogeography, Palaeoclimatology, Palaeoecology*, 255, 4-21.

700 Leckie, R.M., & H.C. Olson, (2003), Foraminifera as proxies for sea-level change on siliciclastic margins,
701 in: Olson, H.C., and R.M. Leckie, eds., *Micropaleontologic proxies for sea-level change and*
702 *stratigraphic discontinuities, SEPM Special Publication No. 75*, 5–19.

703 Lirer, F. (2000). A new technique for retrieving calcareous microfossils from lithified lime
704 deposits. *Micropaleontology* 46, 365-369.

705 Liu, C., & Olsson, R.K. (1992). Evolutionary radiation of microperforate planktonic foraminifera
706 following the K/T mass extinction event. *The Journal of Foraminiferal Research*, 22, 328-346.

707 Lowery, C.M. et al., 2018, Rapid Recovery of Life At Ground Zero of the End Cretaceous Mass Extinction,
708 *Nature* v. 558, p. 288-291, <https://doi.org/10.1038/s41586-018-0163-6>

709 Lowery, C.M. & Fraass, A.J. (2019). Explanation for delayed recovery of species diversity following the
710 end Cretaceous mass extinction. *Nature Ecology and Evolution* [https://doi.org/10.1038/s41559-](https://doi.org/10.1038/s41559-019-0835-0)
711 [019-0835-0](https://doi.org/10.1038/s41559-019-0835-0)

712 Lowery, C.M., Bralower, T.J., Christeson, G., Gulick, S.P.S., Morgan, J.V., and Expedition 364 Scientists
713 (2019). Ocean Drilling Perspectives on Meteorite Impacts. *Oceanography* 32, 120-134.
714 <https://doi.org/10.5670/oceanog.2019.133>

715 MacLeod, K. G., Quinton, P. C., Sepúlveda, J., & Negra, M. H. (2018). Postimpact earliest Paleogene
716 warming shown by fish debris oxygen isotopes (El Kef, Tunisia). *Science*, 360(6396), 1467-1469.

717 Morgan J.V. & 34 others, 2016, The formation of peak rings in large impact craters, *Science* 354, 878-882.

718 Morgan, J.V., S.P.S. Gulick, C.L. Mellet, S.L. Green, & Expedition 364 Scientists (2017) *Chicxulub:*
719 *Drilling the K-Pg Impact Crater, Proceedings of the International Ocean Discovery Program, 364,*
720 *International Ocean Discovery Program, College Station, TX, doi:*
721 *10.14379/iodp.proc.364.103.2017.*

722 Murray, J.W. (1976), A method of determining proximity of marginal seas to an ocean, *Marine Geology*,
723 22, 103–119.

724 Norris, R. D. (1996). Symbiosis as an evolutionary innovation in the radiation of Paleocene planktic
725 foraminifera. *Paleobiology*, 22, 461-480.

726 Okada, H., and Bukry, D. (1980). Supplementary modification and introduction of code numbers to the
727 low-latitude coccolith biostratigraphic zonation (Bukry, 1973; 1975). *Marine Micropaleontology*,
728 5, 321-325.

729 Olsson, R. K., Berggren, W. A., Hemleben, C. I., & Huber, B. T. (1999). Atlas of Paleocene planktonic
730 foraminifera. *Smithsonian Contributions to Paleobiology* 85.

731 Paytan, A., Kastner, M., and Chavez, F.P. (1996). Glacial to interglacial fluctuations in productivity in the
732 equatorial Pacific as indicated by marine barite. *Science*, 274, 1355-1357.

733 Paytan, A., and Griffith, E.M. (2007). Marine barite: Recorder of variations in ocean export productivity,
734 in *Encyclopedia of Paleoclimate and Ancient Environments*, Gornitz, V., Ed., p. 643-651, Springer,
735 New York.

736 Pearson, P.N., Olsson, R.K., Huber, B.T., Hemleben, C., and Berggren, W. A. (2006). Atlas of Eocene
737 Planktonic Foraminifera, Cushman Foundation for Foraminiferal Research Special Publications,
738 vol. 41. Washington, DC, 513.

739 Pedersen, T. F., & Calvert, S. E. (1990). Anoxia vs. productivity: what controls the formation of organic-
740 carbon-rich sediments and sedimentary Rocks?. *AAPG Bulletin*, 74(4), 454-466.

741 Perch-Nielsen, K. (1985). Cenozoic calcareous nannofossils. In Bolli, H.M., Saunders, J.B., and Perch-
742 Nielsen, K. (Eds.) *Plankton stratigraphy*, Cambridge: Cambridge University Press. 427-554.

743 Punekar, J., Mateo, P., & Keller, G. (2014a) Effects of Deccan volcanism on paleoenvironment and planktic
744 foraminifera: A global survey, *Geological Society of America Special Papers*, 505, 91-116.

745 Punekar, J., Keller, G., Khozyem, H., Hamming, C., Adatte, T., Tantawy, A.A., & Spangenberg, J.E.
746 (2014b) Late Maastrichtian–early Danian high-stress environments and delayed recovery linked to
747 Deccan volcanism, *Cretaceous Research*, 49, 63-82.

748 Quillévéré, F., Norris, R.D., Kroon, D., and Wilson, P.A. (2008). Transient ocean warming and shifts in
749 carbon reservoirs during the early Danian. *Earth and Planetary Science Letters*, 265, 600-615.

750 Renne, P.R., Sprain, C.J., Richards, M.A., Self, S., Vanderkluyzen, L., & Pande, K. (2015) State shift in
751 Deccan volcanism at the Cretaceous-Paleogene boundary, possibly induced by impact, *Science*,
752 350, 76-78.

753 Schoene, B., Eddy, M. P., Samperton, K. M., Keller, C. B., Keller, G., Adatte, T., & Khadri, S. F. (2019).
754 U-Pb constraints on pulsed eruption of the Deccan Traps across the end-Cretaceous mass
755 extinction. *Science*, 363(6429), 862-866.

756 Schueth, J. D., T. J. Bralower, S. Jiang, and M. E. Patzkowsky (2015), The role of regional survivor
757 incumbency in the evolutionary recovery of calcareous nannoplankton from the
758 Cretaceous/Paleogene (K/Pg) mass extinction, *Paleobiology*, 41(4), 661-679.

759 Schulte, P. and 40 others, (2010), The Chicxulub asteroid impact and mass extinction at the Cretaceous-
760 Paleogene boundary, *Science*, 327, 1214-1218.

761 Smit, J. and J. Hertogen (1980). An extraterrestrial event at the Cretaceous-Tertiary boundary, *Nature* 285:
762 198-200.

763 Sprain, C. J., Renne, P. R., Vanderkluyzen, L., Pande, K., Self, S., & Mittal, T. (2019). The eruptive tempo
764 of Deccan volcanism in relation to the Cretaceous-Paleogene boundary. *Science*, 363(6429), 866-
765 870.

766 Thunell, R.C. (1976). Optimum indices of calcium carbonate dissolution, in deep-sea sediments. *Geology*,
767 4, 525-528.

768 Troelsen, J.C. (1957). Some planktonic foraminifera of the type Danian and their stratigraphic
769 importance. *US National Museum Bulletin*, 215, 125-131.

770 Van der Zwaan, G.J., Jorissen, F.J. & Stitger, H.C. (1990), The depth dependency of planktonic/benthic
771 foraminiferal ratios: constraints and applications, *Marine Geology*, 95, 1–16.

772 Van Hinsbergen, D.J.J., Kouwenhoven, T.J., & Van der Zwaan, G.J. (2005), Paleobathymetry in the
773 backstripping procedure: correction of oxygenation effects on depth estimates, *Palaeogeography*,
774 *Palaeoclimatology*, *Palaeoecology*, 21, 245–265.

775 Vellekoop, J., Sluijs, A., Smit, J., Schouten, S., Weijers, J.W.H., Sinninghe Damsté, J.S., & Brinkhuis, H.,
776 (2014). Rapid short-term cooling following the Chicxulub impact at the Cretaceous–Paleogene
777 boundary. *PNAS*, 111, 7537-7541.

778 Vellekoop, J., Woelders, L., Açikalin, S., Smit, J., Van De Schootbrugge, B., Yilmaz, I.O., Brinkhuis, H.,
779 & Speijer, R. (2017). Ecological response to collapse of the biological pump following the mass
780 extinction at the Cretaceous-Paleogene boundary. *Biogeosciences*, 14, 885-900.

781 Wade, B.S., Pearson, P.N., Berggren, W.A., & Pälike, H. (2011). Review and revision of Cenozoic tropical
782 planktonic foraminiferal biostratigraphy and calibration to the geomagnetic polarity and
783 astronomical time scale. *Earth-Science Reviews*, 104, 111-142.

784 Zachos, J.C., Arthur, M.A., & Dean, W.E. (1989). Geochemical evidence for suppression of pelagic marine
785 productivity at the Cretaceous/Tertiary boundary. *Nature*, 337, 61-64.

786